Pharmacological activation of the mitochondrial stress protease OMA1 reveals a therapeutic liability in Diffuse Large B-Cell Lymphoma

Adrian Schwarzer[1,2]†, Matheus Oliveira[3]†, Marc-Jens Kleppa[1], Scott D. Slattery[4], Andy Anantha[5], Alan Cooper[5], Mark Hannink[6], Axel Schambach[1], Anneke Dörrie[7], Alexey Kotlyarov[7], Matthias Gaestel[7], Todd Hembrough[5], Jedd Levine[5], Michael Luther[5], Michael Stocum[5], Linsey Stiles[3], Marc Liesa,[3,8]‡*, Matthew J. Kostura[5]‡*

Affiliations:

[1]Institute of Experimental Hematology, Hannover Medical School; Hannover, Germany.

[2]Department of Hematology, Hemostaseology, Oncology and Stem Cell Transplantation, Hannover Medical School; Hannover, Germany.

[3]Department of Medicine, Endocrinology, UCLA, David Geffen School of Medicine at UCLA; Los Angeles, CA, United States.

[4] ScitoVation, Research Triangle Park, NC, United States.

[5]Bantam Pharmaceutical, Research Triangle Park, NC, United States.

[6]Biochemistry Department, Life Sciences Center and Ellis Fischel Cancer Center, University of Missouri; Columbia, MO, United States.

[7]Department of Cell Biochemistry, Hannover Medical School, Hannover, Germany

[8]Institut de Biologia Molecular de Barcelona (IBMB-CSIC), Barcelona, Catalonia, Spain.

† These authors contributed equally

‡ These authors contributed equally

*Corresponding authors. Email: mkostura@bantampharma.com; mlrbmc@ibmb.csic.es

One Sentence Summary (150 characters incl spaces): Selective pharmacological activation of the mitochondrial integrated stress response promotes therapeutic responses in diffuse large B-cell lymphoma

Abstract: (235/250 words)

DLBCL are aggressive, rapidly proliferating tumors that critically depend on the ATF4-mediated integrated stress response (ISR) to adapt to stress caused by uncontrolled growth, such as hypoxia, amino acid deprivation and accumulation of misfolded proteins. Here we show that ISR hyperactivation is a targetable liability in DLBCL. We describe a novel class of compounds represented by BTM-3528 and BTM-3566, that activate the ISR through the mitochondrial protease OMA1. Treatment of tumor cells with compound leads to OMA1-dependent cleavage of DELE1 and OPA1, mitochondrial fragmentation, activation of the eIF2α-kinase HRI, cell growth arrest and apoptosis. Activation of OMA1 by BTM-3528 and BTM-3566 is mechanistically distinct from inhibitors of mitochondrial electron transport, as the compounds induce OMA1 activity in the absence of acute changes in respiration. We further identify the mitochondrial protein FAM210B as a negative regulator of BTM-3528 and BTM-3566 activity. Overexpression of FAM210B prevents both OMA1 activation and apoptosis. Notably, FAM210B expression is nearly absent in healthy germinal-center B-lymphocytes and in derived B-cell malignancies, revealing a fundamental molecular vulnerability which is targeted by BTM compounds. Both compounds induce rapid apoptosis across diverse DLBCL lines derived from activated B-cell, germinal center B-cell, and MYC-rearranged lymphomas. Once-daily oral dosing of BTM-3566 resulted in complete regression of xenografted human DLBCL SU-DHL-10 cells and complete regression in 6 of 9 DLBCL patient-derived xenografts. BTM-3566 represents a first- of-its kind approach of selectively hyperactivating the mitochondrial ISR for treating DLBCL.

INTRODUCTION

Common to all tumors is the need to balance the demands of rapid proliferation with nutrient availability and accumulation of metabolic end products in the tumor microenvironment(*1*). Mitochondria play a key role in altered cancer cell metabolism, cellular stress and survival pathways and are increasingly being considered as targets in cancer(*2–4*). Several Mitochondria Quality Control (MQC) pathways serve to maintain the integrity of mitochondria. MQC pathways sense changes in mitochondrial oxidative phosphorylation, membrane potential, proteostasis and translation of mitochondrial DNA encoded proteins (*5–7*). MQC pathways signal to cytosolic pathways that control the ATF4-Integrated Stress Response (ISR), an adaptive gene expression program controlling amino acid biosynthesis and transport, redox homeostasis and enhanced protein folding (*5*, *8*, *9*). The ATF4-ISR facilitates adaptation to the tumor microenvironment and is shown to be a pharmacologically targetable tumor dependency (*2*, *10*). Activation of the ISR is initiated by phosphorylation of the translation initiation factor eIF2α, which leads to a decrease in protein synthesis and increased activity of the nuclear transcription factors ATF3, ATF4, ATF5 and DDIT3 (*11–14*). The ISR is normally self-limiting as biosynthesis of an eIF2α specific phosphatase (PPP1R15A) is upregulated, leading to dephosphorylation of eIF2α and restoration of normal protein synthesis (*15–18*). Persistent ISR activation, however, can sensitize cells to apoptotic stimuli by altering the levels of pro- and anti-apoptotic proteins (*19–24*).

Herein we describe the preclinical pharmacology of a novel class of pyrazolo-thiazole derivatives, first described for their ability to induce cell growth arrest and cell death in a wide variety of solid and hematopoietic tumor cell lines (*25*). We demonstrate that BTM compounds specifically hyperactivate the ISR through activation of the mitochondrial MQC protease OMA1, thereby shifting the equilibrium from ATF4-ISR controlled pro-survival effects towards tumor cell death. Sensitivity to the compounds is suppressed by the presence of a mitochondrial protein, FAM210B, which is minimally expressed in DLBCL to explain the sensitivity of DLBCL to BTM compounds.

RESULTS

BTM-compounds selectively kill DLBCL *in vitro*. We previously described a series of pyrazolo-thiazole compounds that displayed anti-proliferative activity across a range of hematopoietic and solid tumor cell lines (*29*). We sought to further improve this class of compounds by optimizing the substituents around the pyrazolo-thiazole core. This effort yielded two lead compounds, BTM-3528 and BTM-3566. A structure-activity relationship is highlighted with a closely related, but inactive compound, BTM-3532 (**Fig. 1A**). The anti-proliferative activity of BTM-3528 and BTM-3566 were compared in a panel of 99 tumor cell lines, including 19 hematopoietic lines and 80 solid tumor lines (**Fig. 1B,C** and **Supplemental Table S1**). BTM-3528 and BTM-3566 demonstrated equivalent activity across select solid tumor cell lines, with greater activity observed in lung and colorectal, than in skin or breast cancer cell lines **(Fig. 1C, Supplemental Table S1)**. (**Fig. 1B**, **Supplemental Table S1**). In contrast, hematopoietic tumor lines were broadly responsive to both BTM compounds (**Fig. 1B Supplemental Table S1**) with the most sensitive being Burkitt Lymphoma and DLBCL. A comparison of BTM-3528 and BTM-3566 revealed an equivalent spectrum of activity against DLBCL lines of diverse genotypes, including *MYC*-rearranged ("double" and "triple" hit) lymphomas, with >90% growth inhibition and IC_{50} values of 0.16-0.57 μM (**Supplemental Table S2**). BTM-3528 and BTM-3566 induced caspase 3/7 and apoptosis in all tested B-cell lymphoma lines, but not in tested solid tumor lines (**Figure 1D, and Supplemental Fig. S1**), which exhibit cell growth inhibition and G1 arrest, but not apoptosis (**Supplemental Fig. S2**).

BTM-3566 has robust *in vivo* activity in both human cell line and patient derived xenograft models. The robust *in vitro* efficacy observed with BTM-3528 and BTM-3566 led to an evaluation of activity *in vivo* in cell-line derived and patient-derived xenograft models. Pharmacokinetics and oral bioavailability of BTM-3566 was established with i.v./p.o. crossover studies in mice (**Supplemental Fig. S3**) and was found acceptable for once daily oral dosing. BTM-3566 was first tested in a human xenograft model using the double-hit lymphoma DLBCL tumor line SU-DHL-10. At the 10 mg/kg dose, we observed an early decrease in tumor growth rate that was lost with further dosing (**Fig. 2A upper panel**). However, at doses at or above 20 mg/kg, a Complete Response (CR, defined as no palpable tumor) was observed in all animals by 10 days of dosing and maintained for 21 days of dosing (**Fig. 2A upper panel**). Thirty-day tumor free survival was

maintained in 40% of animals dosed with 20 mg/kg and 60% of animals dosed with 30 mg/kg BTM-3566 (**Fig. 2A upper panel**). Mean weight loss in mice dosed with 20 mg/kg daily of BTM-3566 po, qd for 21 days was < 5% with a maximum observed weight loss of <10% in any individual mouse (**Fig. 2A lower panel**). In the 30 mg/kg dose group, two of 10 mice exceeded 20% body weight reduction, necessitating an unscheduled dose holiday.

We further tested BTM-3566 in 9 human DLBCL patient-derived xenograft (PDX) models representing ABC- and GCB DLBCL-subtypes and including high-risk genotypes (**Fig. 1C**). Treatment with 20 mg/kg of BTM-3566 resulted in robust efficacy with marked growth inhibition observed by day 21 in 100% of animals in all tumor models tested **(Fig. 2B, C**). A Complete Response occurred in 7 of the 9 PDX models, with 6 models having CR in all mice (100%). When pooling the 27 mice in the treatment arms of the nine models, CR was observed in 66% (19 of 27) of all mice. Partial Response (PR) occurred in another 4 mice. Two mice had stable tumors, and two mice had a tumor modestly greater than the starting baseline tumor volume of 200mm^3. In summary, the overall response rate (CR+PR) was 85.2 % with stable disease in the remaining 14.8% of treated animals. (**Fig. 2B**).

BTM compounds induce activation of the ATF4-linked integrated stress response. To shed light on the mechanism of action of the active compounds, we performed RNA sequencing (RNA-seq) in HCT-116 cells treated with BTM-3528 (at 10, 1, 0.1 μM) for 1, 2, 4, 6, and 8 hours and in untreated cells. Treatment with BTM-3528 induced rapid changes in gene expression, with differentially expressed genes appearing at the 4-hour time point (**Fig 3A**). Gene set enrichment analysis revealed a strong upregulation of genes associated with the ATF4-linked integrated stress response (**Fig. 3B**). Consistently, most upregulated genes at each time point were direct ATF-4 target genes (**Fig. 3A,** in red font). GSEA results implicated three kinases, HRI (EIF2AK1), sensing mitochondrial stress, GCN2 (EIF2AK4), sensing amino acid depletion and PERK (EIF2AK), sensing endoplasmic reticulum (ER-) stress as potential drivers of BTM-3528 mediated ATF4 gene expression. Since ER-stress also activates the transcription factors ATF6 and XBP1s independently of the activation of PERK, we determined whether ATF6 and XBP1 target genes were affected by BTM-3528 treatment. We found that genes specifically regulated by ER-stress and the transcription factors ATF6 or XBP1 (*26*) were not robustly upregulated by treatment with BTM-3528 (**Fig. 3C, left and middle panel**), suggesting that PERK and ER-stress do not play a role in the BTM-3528 mediated induction of ATF4-regulated genes. Gene set enrichment analysis

revealed that transcriptional changes induced by BTM-3528 treatment were highly similar to those observed in the context of mitochondrial stress (*8*) (**Fig. 3C, right panel**).

BTM-3528 induced ATF4-regulated gene expression was confirmed in cells with different tissues of origin. (**Fig. 3D**). BTM-3528 induced ATF4-regulated gene expression in the solid tumor lines A549 and HCT116, in the chronic myelogenous leukemia cell line HAP1, and in two DLBCL cell lines SU-DHL-2 and SU-DHL-10. ATF4-regulated genes were not induced in nonresponsive normal human lung fibroblasts. Consistent with the RNASeq data, the transcriptional response was selective for ATF4, as no ATF6- or ERN1/Xbp1-regulated transcripts were induced by BTM-3528 **(Fig. 3D**).

To determine whether the ISR was activated at the protein level, we determined the extent of phosphorylation of eIF2α and ATF4 protein expression in HCT-116 cells treated with BTM-3528. Western blotting demonstrated a time-dependent increase in eIF2α phosphorylation (**Fig. 3E**) while immunofluorescent staining of ATF4 revealed a dose- and time-dependent accumulation of ATF4 protein in the nuclei of HCT-116 cells treated with BTM-3528 (**Fig. 3F and Supplemental Fig. S4**). Induction of ATF4 by BTM-3528 occurred within 1 hour following treatment with an EC_{50} of 0.19 μM. We confirmed these results in BJAB cells, which demonstrated increased phosphorylation of eIF2α accompanied by ATF4 upregulation upon exposure to BTM-3528 (**Fig. 3G**).

BTM-3566 activates the eIF2α ATF4-ISR *in vivo.* We next tested the ability of BTM-3566 to induce the eIF2α–ATF4-ISR *in vivo* in our SU-DHL-10 xenograft model of DLBCL. Mice were dosed with 3, 10, and 30 mg/kg per day of BTM-3566 for 5 days with tumor volumes recorded and tumors sampled for biomarker analysis. Six hours following drug administration the expression of ATF4 target genes (ASNS, DDIT3, TRIB3 and CDKN1A) increased severalfold in a dose-dependent manner **(Supplemental Fig. S5)**. Both the reduction in tumor volume and the increase in ATF4 target gene expression for ASNS, CDKN1A, TRIB3 and DDIT3 were correlated to overall BTM-3566 exposure in the mouse (**Supplemental Fig. S5**). Taken together, these data demonstrate that BTM compounds trigger the ATF4-linked integrated stress response at the transcriptional and the protein level and that *in vitro* activation of the ATF4-ISR by BTM-3566 is retained *in vivo* and correlates with efficacy in a human DLBCL xenograft model.

BTM-3528 induces OMA1 dependent mitochondrial fragmentation. Several recent studies have shown that agents which depolarize mitochondria, deplete cells of ATP or otherwise affect mitochondrial quality or structure can induce ATF4 via activation of the mitochondrial protease OMA1 (*8*, *27*, *28*). Consequently, we assessed the effects of BTM-3528 on mitochondrial structure in HCT-116 cells. Parental and OMA1 -/- HCT-116 cells were treated with 3 μM BTM-3528, stained with Mitotracker Green and live-cell imaged. BTM-3528 induced a significant reduction in both mitochondrial aspect ratio and form factor in parental, but not in OMA1 -/- cells (**Fig. 4A, B).** The data suggest that BTM-3528 disrupts mitochondrial network morphology in an OMA1 dependent manner.

BTM-compounds activate OMA1 proteolytic activity. Mitochondrial fragmentation can be associated with cleavage of proteins that are required for maintenance of a fused state. OPA1 is a dynamin-like protein that controls inner membrane fusion and cristae shape, with 5 isoforms detected by Western blot (bands a-e). OPA1 isoform content is sensitive to OMA1 activation. OMA1 activation cleaves the long isoforms of OPA1 (L-OPA1) to short OPA1 isoforms (S-OPA1), resulting in mitochondrial fragmentation (*29–32*). L-OPA1 levels were reduced >90% in parental HCT-116 cells, but not in OMA1 -/- HCT-116 cells following 4 hours of exposure with 3 μM BTM-3528 or BTM-3566, but not inactive BTM-3532 (**Fig. 4D, E).** L-OPA1 levels were significantly reduced as early as 30 minutes after active BTM compound treatment, as shown by the decrease in the high molecular weight isoform of OPA1 (L1-OPA1) in parental HCT116 cells (**Fig. 4F, G**). Notably, in this solid tumor line, apoptosis does not occur, suggesting that OMA1 activation and cleavage of OPA1 is not sufficient to induce subsequent release of cytochrome c and activation of the intrinsic apoptotic pathway.

Mitochondrial membrane depolarization or electron transfer blockage are not responsible for OMA1 activation induced by BTM compound treatment. The most well described mitochondrial insults preceding OMA1 activation involve a decrease in mitochondrial ATP production, either achieved by depolarization/uncoupling or by blocking electron transfer (*32–34*). Therefore, we determined whether BTM compounds could depolarize mitochondria or directly inhibit electron transfer. Parental and HCT-116 OMA1 -/- cells were treated with BTM-3528, BTM-3566 or the inactive analogue BTM-3532 for 3 hours. Live cells were then stained with TMRE and MTG and then visualized using confocal microscopy. While the mitochondrial

uncoupler FCCP strongly reduced the TMRE/MTG ratio, BTM compounds had no effect, consistent with a lack of mitochondrial depolarization (**Fig. 4C**).

To further evaluate effects on mitochondrial function, we determined whether acute changes in basal oxygen consumption rate (OCR) occurred in cells treated with BTM compounds. After 30 minutes of treatment with BTM-3528 or BTM-3566 in parental cells, no significant changes occurred in OCR (**Fig. 4H, I).** ATP-linked respiration and bioenergetic efficiency were mildly decreased and further reduced by 4 hours of treatment with BTM compound in parental HCT-116 cells, but not in OMA1 KO cells (**Fig. 4I, J; Supplemental Fig. S6A, B).** These data suggest that BTM compound-mediated effects on respiration are dependent on the presence of OMA1 and do not result from direct inhibition of electron transport or uncoupling of mitochondrial respiration.

OMA1 dependent cleavage of DELE1 leads to HRI activation and apoptosis. Recent work has demonstrated that activation of OMA1 leads to proteolytic cleavage of DELE1 and subsequent release of peptide fragments from the mitochondria to the cytosol, which bind to and activate HRI **(See Fig. 5A**; ref.(*27*, *28*)). On the other hand, it has also been suggested that OPA1 processing and mitochondrial fragmentation can induce or facilitate apoptosis. To assess the role of OMA1, DELE1 and OPA1 as effectors of BTM-3528 and BTM-3566 activity in DLBCL, we created clonal BJAB cell lines with homozygous deletions of OMA1 or DELE1, or where the OMA1-cleavage site in L-OPA1 was deleted ($OPA1^{\Delta S1/\Delta S1}$). BTM-3566 failed to induce OPA1 cleavage in $OMA1^{-/-}$ cells and in $OPA1^{\Delta S1/\Delta S1}$ cells. In contrast, deletion of DELE1 did not affect OPA1 processing **(Fig. 5B).** Phosphorylation of eIF2α and induction of ATF4 protein was found to be dependent on the presence of OMA1 and DELE1, but not on cleavage of OPA1 (**Fig. 5B**). Functionally, deletion of either OMA1 or DELE1 protected BJAB cells from BTM-3566 and BTM-3528 induced apoptosis (**Fig. 5C, Supplemental Fig S7A**). In contrast, the $OPA1^{\Delta S1/\Delta S1}$ BJAB cell line remained fully sensitive to BTM-3566 and BTM-3528-induced apoptosis (**Fig. 5C. Supplemental Fig S7C**). Thus, activation of OMA1 is required for BTM-3566 and BTM-3528-induced activation of the ISR and apoptosis via cleavage of DELE1, whereas OMA1- mediated processing of OPA1 was dispensable for the therapeutic effect of BTM.

HRI activation leads to apoptosis in DLBCL cells. Our data are consistent with the work of Guo (*27*) and Fessler (*28*), which established the central role of HRI, and OMA1 and DELE1, but not OPA1 in mitochondrial stress-mediated ATF4 protein expression. To test the dependency of compound action on HRI activation, we created an HRI -/- BJAB cell line using CRISPR gene

editing. Following treatment with 2 μM BTM-3566 or BTM-3528, neither phosphorylation of eIF2α nor increased ATF4 protein was observed in HRI -/- cells (**Fig. 5D, Supplemental Fig 7B**). We used CRISPR/Cas9 to create ATF4-/- BJAB cells, as well as eIF2α -S49A/S52A double mutant BJAB cells, in which the serine residues phosphorylated by activated HRI were mutated to alanine. Following treatment with BTM-3528, ATF4 protein expression was not observed in BJAB cells containing the eIF2α double mutation. The functional consequences of these mutations on apoptosis were assessed using Annexin/propidium iodide staining followed by FACS analysis. Parental BJAB cells undergo apoptosis within 12 h of exposure to 3 μM BTM-3528 (Fig. 5E). HRI-/- cells and the eIF2α -S49A/S52A cells were resistant to BTM-3528-induced apoptosis, as were ATF4-/- cells. By 48 hours post-treatment, no viable parental BJAB cells remained, but HRI-/- and eIF2α -S49A/S52A cells remained largely viable (**Fig. 5E; Supplemental Fig. 7C**). We hypothesized that the effect of eIF2α phosphorylation on survival might be related to suppression of translation of short-lived proteins essential for cancer cells. Polysomes from parental and ATF4-/- BJAB cells exhibited a significant shift towards smaller size, while knockout of HRI or mutation of eIF2α preserved polysome size, consistent with an inability to translate ATF4 protein or induce cell death (**Fig. 5F- I**).

The mitochondrial protein FAM210B suppresses BTM compound activity. A panel of 407 cell lines were screened to identify mutational and transcriptional associations with BTM-3528 compound activity (**Supplemental Fig. S7**). Each cell line was treated in duplicate with BTM-3528 to establish a dose response. The activity area (Area Under Curve, AUC) for each dose response was then computed (**Supplemental Table S3**). The AUC response data was analyzed for correlation to genomic alterations or gene expression levels in The Cancer Cell Line Encyclopedia (*35*). No genomic alterations were associated with compound activity. Rather, expression of several genes was associated with compound activity in both hematopoietic and solid tumors. Specifically, expression of FAM210B was strongly correlated with response to BTM-3528 across all cell lines tested (**Fig. 6A, Supplemental Tables S4, S5**). Mean FAM210B expression levels are significantly lower in drug-sensitive cell lines (**Fig. 6B**). Notably, the most responsive cell lines are derived from B-cell lymphomas (DLBCL, Burkitt's and Mantle cell lymphoma) and have the lowest levels of FAM210B expression (**Fig. 6C**).

To determine if increased FAM210B expression suppresses BTM compound activity, BJAB cells that stably express FAM210B-tGFP were prepared and compared to parental BJAB and BJAB HRI -/- cells. Each cell line was tested for response to BTM-3532, BTM-3528 and BTM-3566. Bortezomib and FCCP were included as controls to assess the specificity of FAM210B on preserving cell viability when ATF4 ISR is induced via alternative methods of activation. FAM210B-tGFP expression significantly suppressed the activity of BTM-3528 and BTM-3566 but had no effect on bortezomib or FCCP-induced cell death **(Fig. 6D).** Importantly, KO of HRI reduced the activity of both bortezomib and FCCP, confirming the common utilization of HRI in induction of the ATF4 ISR and subsequent apoptosis.

To determine the effects of FAM210B on OMA1 activation we compared the ability of the BTM-3528, 3566 and the inactive control BTM-3532 to activate OMA1 in the presence or absence of FAM210B-tGFP overexpression. As expected, L-OPA1 cleavage in parental HCT-116 cells was observed in the presence of the BTM-3528 and BTM-3566 but not BTM-3532 (**Fig. 6E**). L-OPA1 cleavage did not occur in HCT-116 cells stably expressing FAM210B-tGFP (**Fig. 6F**), indicating that FAM210B acts distal to OMA1 to suppress the effect of BTM compounds on OPA1 cleavage. FCCP-induced cleavage of OPA1 was unaffected by FAM210B-tGFP. We also compared the effects of FAM210B expression on ATF4 protein expression using BTM-3566 and alternative inducers of the ATF4 ISR. FAM210B expression robustly suppressed ATF4 induction by BTM-3566 but not by amino acid starvation, tunicamycin, bortezomib or ONC201 **(Supplemental Fig. 8).** These data demonstrate that the mitochondrial inner membrane protein FAM210B uniquely regulates activation of OMA1 by the BTM compounds but not by other inducers of the ATF4 ISR. We next determined whether FAM210B could prevent OMA1 activation and its downstream effects on mitochondrial respiration in HCT116 cells. We found that BTM compound-dependent decreases in basal, ATP-linked, and maximal mitochondrial respiration were blocked in cells overexpressing FAM210B-tGFP (**Supplemental Fig. S9A and 9B**). Collectively, the data demonstrate that the mitochondrial inner membrane protein FAM210B suppresses OMA1 activation by BTM compounds-and prevents consequential effects on mitochondrial structure, function, cell growth and cell survival.

DISCUSSION

Tumors develop characteristics to grow in a manner unfettered from normal growth control (*36*). Mitochondria play a crucial role in this process as central hubs controlling cell survival in response to proapoptotic stimuli signaling through mitochondria to activate the intrinsic apoptotic pathway(*37*). Our data support the hypothesis that BTM compounds activate the mitochondrial protease OMA1, leading to activation of HRI, phosphorylation of eIF2α and induction of the ATF4-ISR. DLBCL tumors appear particularly sensitive to the action of BTM compounds, undergoing apoptosis *in vitro* and exhibiting profound regression *in vivo*. Importantly, therapeutic activity of the BTM compounds appears to work independently of genomic background and spans a breadth of DLBCL subtypes based on cell-of-origin, presence of MYC rearrangements and other genetic alterations. These results highlight a clinical approach that will benefit a heterogenous group of patients with relapsed/refractory DLBCL, who are not suitable for or have failed high dose chemotherapy or stem cell transplantation and patients who fail CAR-T-cell therapy.

BTM compounds activate the mitochondrial protease OMA1, leading to apoptosis in DLBCL tumor lines *in vitro* and tumor regression *in vivo*. Activation of the apoptotic program is dependent on OMA1-dependent cleavage of DELE1, which leads to activation of HRI and the eIF2α–mediated ATF4 ISR. The downstream consequences of eIF2α phosphorylation and ATF4 ISR activation are twofold: there is a global inhibition of translation linked to eIF2α phosphorylation, and an ATF4-dependent induction of its downstream targets (e.g., ATF3, DDIT3, etc.). Both events play a role in the observed therapeutic outcome. Mutations or deletions of all components in the pathway leading to eIF2α phosphorylation phenocopy each other, as loss of OMA1, DELE1, and HRI, as well as a double mutant of eIF2α that prevents phosphorylation of Ser 49 and Ser52, all suppress BTM-induced apoptosis. The effects on global translation may be related to the reduction in proteins involved in cell survival. Critical oncogenic proteins with short half-lives such as MYC, CCND3 and MCL1 may be significantly reduced in DLBCL cells treated with BTM-3528. Similarly, our data also support a role for ATF4-regulated gene transcription in the apoptotic response induced by BTM compounds. Although the particular ATF4-dependent events associated with apoptosis induced by BTM compounds are not fully understood, the ATF4 target gene DDIT3 (CHOP) is known to promote cell death through a variety of mechanisms in the context of the ER-stress response (*38–41*).

Activation of OMA1 also results in cleavage of OPA1, a dynamin like protein involved with the fusion of the inner mitochondrial membrane, cristae structure and mitochondrial morphology (*29–31*). Controlled OMA1-dependent proteolysis of L-OPA1 to S-OPA1 appears to be an early event associated with cristae remodeling (*32*, *42–45*). Deletion of the canonical OMA1 cleavage site in OPA1 failed to alter the timing or extent of apoptosis in BJAB cells treated with BTM-3528. Likewise, there was no impact on the activation of HRI, eIF2α phosphorylation or induction of ATF4 protein. This result suggests that OMA1-dependent OPA1 cleavage is neither necessary nor sufficient to activate apoptosis induced by BTM compounds. This observation agrees with our data showing that eIF2α phosphorylation is the major event initiating apoptosis in DLBCL cell lines. Such a result is consistent with BTM compounds not being mitochondrial toxins or directly promoting mitochondrial permeability transition pore opening.

Screening of 406 tumor cell lines with BTM-3528 and an analysis against the CCLE database revealed no mutations correlated with response to BTM-3528. Rather the expression of a subset of genes appeared to correlate with response to compound. The strongest correlation was with the mitochondrial protein FAM210B, where increased expression was correlated with decreased responsiveness to compound. FAM210B is not expressed or is expressed at low levels in most hematopoietic malignancies, particularly B-cell malignancies. Tellingly, DLBCL lines, which are the most sensitive, do not express FAM210B to any extent. Low expression of FAM210B in DLBCL is related to the observation that normal human germinal center B-cell centrocytes and centroblasts do not express FAM210B (**Supplemental Fig. 11**) (*46*). Increased expression of FAM210B in both BJAB and HCT116 cells provides specific resistance to BTM compound-induced activation of the ATF4 ISR while having no effect on other inducers of the ISR (tunicamycin, nutrient deprivation and bortezomib) or compounds that affect mitochondrial proteostasis (mitochondrial uncouplers and ONC201). As such, there must be multiple pathways inside mitochondria that, when perturbed, lead to activation of the ATF4 ISR but only a FAM210B-regulatable process is affected by BTM compounds.

FAM210B is a mitochondrial inner-membrane protein involved in high-capacity heme biosynthesis occurring during erythropoiesis, acting to increase the importation of iron into the mitochondria (*47–49*). FAM210B may have broader activity controlling cellular metabolism unrelated to heme biosynthesis but tied to its ability to act as a scaffold protein for other

mitochondrial membrane or matrix proteins. Reduction in FAM210B expression using siRNA leads to increased mitochondrial respiratory capacity, decreased glycolysis and an aggressive metastatic tumor phenotype (*50*). FAM210B has also been described as a tumor suppressor with lower FAM210B levels associated with poor prognosis in patients with renal, cervical and lung cancers, (*50, 51*).

Induction of eIF2α phosphorylation and the ATF4 ISR is increasingly being viewed as a clinically valid approach to anti-cancer therapeutics. For example, the 26S proteasome inhibitor bortezomib relies on activation of HRI to phosphorylate eIF2α, with subsequent induction of ATF4 and CHOP (*52, 53*). ONC201, a compound being tested in clinical trials for multiple myeloma and glioblastoma (*54–56*), induces G1 cell cycle arrest, eIF2α phosphorylation, ATF4 ISR and CHOP via activation of the mitochondrial protease CLPP1. Collectively, the biological activities of the BTM compounds, bortezomib and ONC201 support the hypothesis that persistent induction of the ATF4 ISR in tumor cells can be maladaptive, leading to cancer growth arrest and apoptosis (*57–60*).

MATERIALS AND METHODS

Cell line compound testing. Screening of 406 cell lines was performed by Crown Bioscience (OmniScreen Platform). The protocol estimated the growth of each cell line from the initial plating density. Cells were plated at a starting density of 4×10^3 cells/well and incubated for 24 hours. BTM-3528 was prepared as a 10×solution of test article with a final working concentration of 30 µM of test article in media with nine 3.16-fold serial dilutions, following addition of BTM-3528, the plates were incubated for 96 hours at 37°C with 5% CO2. Final cell numbers were determined using the Cell-Titre Glo assay (Promega). The absolute IC_{50} (EC_{50}) curve was fitted using nonlinear regression model with a sigmoidal dose response.

Caspase 3/7 activity was determined following treatment of cells with BTM-3528 or BTM-3566. using the Caspase-Glo® 3/7 assay (Promega).

Cell viability in BJAB cells was determined by staining cells to detect all nuclei (Hoechst 33342), apoptosis (Annexin V Alexa Fluor 647), and dead cells (YOYO-1). The cells are imaged using confocal microscopy (Opera Phenix), and classified as live, apoptotic, or necrotic. Total live cells, percent apoptotic and percent dead, are determined for each well.

Annexin V Apoptosis Assay To quantify apoptosis, BJAB cells were cultivated in a 96-well format and treated with BTM compounds for the indicated time intervals. Cells were washed twice with ice cold PBS and resuspended in 1x Binding Buffer (BD Biosciences) at a concentration of 1 x 10^6 cells/ml. To 0.5 x 10^5 cells 2.5 µl of Annexin V-APC or Annexin V-FITC (BD Bioscience) were added and incubated for 15 min at RT in the dark. Cells were washed once with Binding Buffer and the pellets were resuspended in 100 µl Binding Buffer containing either 2 µl PI (50 µg/ml) or 2 µl DAPI (1 mg/ml). Cells were analyzed on a Cytoflex S (Beckman Coulter).

Transcriptomic Profiling: The human colon adenocarcinoma cell line HCT116 was used to evaluate the effects of BTM compounds on gene expression. To fully evaluate the effects of the compound on cell-cycle controlled genes, cells were synchronized prior to BTM compound treatment. HCT-116 cells were first blocked in S phase by treatment with thymidine. After 24 hours, the thymidine containing media was removed and replaced with media containing nocodazole to block cells in M phase in a high degree of synchrony. Cells were then released into G1 either in complete medium or complete medium plus 10, 1, or 0.1 µM BTM-3528. Cells were harvested at five time points: 1, 2, 4, 6, and 8 hours after release into G1 phase, and mRNA

extracted for Illumina RNA-seq. Three replicates of each concentration and time point along with time point specific controls (i.e., cells without compound) were collected for sequencing.

RNAseq Data Analysis. FASTQ files contain the read pairs for a sample along with their base pair quality score. Quality scores are based on the PHRED33 scoring scheme. Illumina RNA-seq read files (FASTQ files) were assessed with FASTQC for read quality (www.bioinformatics.babraham.ac.uk/projects/fastqc/). Quality scores were used to trim the leading and trailing base pairs to retain only those with a minimum PHRED quality score of 30 or better, and with a minimum retained read length of 75bp.(*61*) Read pairs were mapped with BOWTIE2 to the indexed version of human genome build USCS hg38 (support.illumina.com/sequencing/sequencing_software/igenome.html) using a local sensitivity mapping algorithm with one allowed base pair mis-match (*62*). The resultant SAM files were converted to BAM format and counted with the Python tool HTSeq.(*63*) Each read pair was counted once per annotated genomic feature. The genomic feature count matrix was analyzed using R 4.1.2 (*64*) and Bioconductor 3.14 (*65*). Filtering and normalization were performed using the R package edgeR (*66*). The complete count table was filtered to retain genes with at least 10 reads (lcpm > 0.6) in at least 15 samples resulting in 14,287 retained genes. The filtered counts were normalized using the trimmed mean of M-values normalization procedure. Differentially expressed genes were computed using limma-voom (*67*). For each time points we computed the Toplists (differentially expressed genes) for the following contrasts: ”(BTM 10µm and BTM 1µM) vs. DMSO”. The final output of limma-voom is a table of Log_2 fold change, p-values for the defined contrasts tested, as well as Benjamini-Hochberg corrected false discovery p-values (FDR) (*68*). Volcano plots were generated in R using EnhancedVolcano. For gene set enrichment analysis (GSEA) the log2-FC between BTM treated (10µm and 1µM) versus DMSO treated samples were computed for all 14,287 genes using limma-voom for each time point. These 14,287 log2-FC values were subsequently analyzed with the Broad GSEA tool using GSEA (*69*)-preranked with the permutation type set to Gene set (1,000 permutations). The gene sets tested for enrichment were from MSigDB.v7.5.1 (C2- canonical pathways gene sets). Gene sets smaller than 15 genes or larger than 300 genes were filtered out, resulting in 1762 gene sets that were tested for each ranked gene list. (All data and analysis can be found in Supplemental Table S6: file RNASeq_BTM3528_Data and Analysis)

RNA Extraction and QPCR. For tissue isolated from xenograft models, the tumor was excised, weighed and placed into RNALater (ThermoFisher) and frozen. Thawed tissue was homogenized using metal beads. RNA was extracted using QIAGEN RNeasy midi kit according to the instructions. RNA was reverse transcribed to cDNA (Applied Biosystems – High-Capacity RNA-to-cDNA kit). qPCR was carried out using Applied Biosystems TaqMan™ Fast Advanced Master Mix with Taqman gene expression assays on an ABI 7900HT Real Time PCR machine using a standard protocol.

Xenograft models. Human cell line xenograft models were established using SU-DHL-10 cells (DSMZ). Cells were grown in RPMI 1640 supplemented with 10mM HEPES buffer, /L-Glutamine, 1mM Na pyruvate, 4500 mg/L Glucose, 15% Non-Heat-Inactivated Fetal Bovine Serum and Penicillin/Streptomycin. Cells were harvested by centrifugation and resuspended in cold 50% serum-free medium: 50% Matrigel to generate a final concentration of 2.50E+07 trypan-excluding cells/mL. Female Envigo SCID beige mice (C.B-17/IcrHsd Prkdc^{scid}lyst^{bg-j}) were implanted subcutaneously high in the right axilla on Day 0 with 5x10^{6} cells/mouse. Mice were randomized into study groups based on tumor volume with a mean tumor burden for each group of 150mm^{3}. BTM-3566 was prepared as a solution in dosing vehicle containing 5% NMP, 15% PEG400, 10% Solutol, and 70% D5W. All mice were dosed once daily by oral gavage for 21 days. The final dose concentration was 4 mg/ml, and the dose volume was 5 μL /gram. Tumor volume and body weights were determined every 3rd day. All mice were dosed according to individual body weight on the day of treatment.

Patient derived xenograft models were performed at Crown Biosciences. Tumor were implanted in Balb/c nude (LY0257); NOD SCID (LY2214, LY2264, LY2345, LY3604, LY6701) or NPG/NOD/SCID (LY6933, LY6934) mice. Each mouse was inoculated subcutaneously in the right flank region with fresh tumor derived from mice bearing established primary human cancer tissue. Mice were randomized into a vehicle or treatment group with a mean tumor burden of 200 mm^{3}. All mice were dosed once daily by oral gavage for 21 days. Tumor volume and body weights were determined three times per week.

Confocal live cell imaging

HCT-116 cells were plated in a 35 mm dish containing a 14 mm, uncoated coverslip (MatTek). The next day, cells were stained with McCoy media containing 200nM Mitotracker green (MTG)

and 15nM of tetramethyl rhodamine, ethyl ester (TMRE) for 40 minutes. Cells were then treated with 3µM BTM-3528 or 4µM FCCP in McCoy containing 15nM TMRE, but lacking MTG, and incubated for 3h. Imaging was perfumed using a 63x objective and in a Zeiss LSM880 confocal microscope with Airyscan mode.

Mitochondrial membrane potential

Cells were plated in black clear-bottom 96 wells plate and stained with McCoy media containing 200nM MTG and 15nM of TMRE for 40 minutes. Cells were then treated with 3µM BTM-3528 or 4µM FCCP in McCoy containing 15nM TMRE, but lacking MTG, and incubated for 30 minutes. MTG and TMRE signal was obtained by imaging in two wavelengths (MTG – Excitation 460-490 nm and Emission 500-550 nm; TMRE – Excitation 560-580 nm and Emission 585-605 nm) using a PerkinElmer Operetta microscope system with 40x lens. Five fields of each well were analyzed and TMRE/MTG fluorescence ratio was determined by image processing with Harmony software.

Image analysis

Mitochondrial morphology was assessed using Fiji/ImageJ software and a Trainable Weka Segmentation plugin. Mitochondrial membrane potential, TMRE/MTG fluorescence ratio was calculated from segmented mitochondrial structures obtained by MTG channel. One-way ANOVA and Tukey's multiple comparison test were used for statistical analysis; P-values ≤ 0.05 (*) were considered significantly different.

Mitochondrial Respirometry

Respirometry assays were run on a Seahorse Extracellular Flux Analyzer (Agilent). HCT116 cells were seeded at 14,000 cells/well using XF96 well microplates and incubated overnight (37°C and 5% CO2) in McCoy's 5a Modified Medium culture medium with 10% FBS. Before the respirometry assay, cells were washed with assay medium: DMEM with 10mM glucose, 2mM glutamine, 1mM pyruvate, 5mM HEPES, and 10% FBS (pH 7.4). BTM compounds were tested at a final concentration of 3µM, and cells were either acutely treated during the assay or pretreated for 4 hours before the assay. In pretreatment experiments, compounds were added in complete medium and incubated at 37°C and 5% CO2. Compounds injected during the assay included 2µM oligomycin, 1µM FCCP, and 2µM of antimycin A and rotenone. Upon completion of each

respirometry assay, the cells were stained with 1µg/mL Hoechst and cell number was measured with an Operetta High-Content Imaging System. The respirometry well level data (pmol O2/min) was normalized to cell number per well (pmol O2/min/10^3 cells) in each assay.

Mutagenesis of BJAB cells. BJAB cells were obtained from the German Collection of Microorganisms and Cell lines (DSMZ #ACC 757). Alt-R crRNA, Alt-R tracrRNA and Alt-R Cas9 Nuclease V3 were purchased from IDT. The genomic crRNA target sequences were: ATF4: 5'- GCGGGCTCCTCCGAATGGC-3', HRI: 5'- ATAGTCGAGAGAAACAAGCG-3', eIF2S1: 5'- TTCTTAGTGAATTATCCAGA-3', OMA1: 5'-CTGGAAGTAAGTCCAATCAC-3', OPA1: 5'-GCGTTTAGAGCAACAGATCG-3', DELE1(knock-in):5'-GAAAGGAGTGTTGTAAGACT-3', DELE1 (knock-out): 5'-ACTGGGACCTAGCCTCTGGA-3'. For HDR-mediated knock-ins IDT ultramers with the following sequences were used as DNA donors. The base substitutions introduced for mutation of S49 and S52 are in **bold capitol**: 5'-a*c*ttacctttttctttgtccaccctaatgacaaccacacactcattcctgccaattcggatgagtttgttgatagaacggatacgtcttct**TGC**taattc**TGC**aagaagaatcatgccttcaatg*t*t-3'. For the knock-in of a HA-tag into the DELE1 locus the following template was used with the HA-tag and linker in uppercase: 5'-t*g*gaaagggttgctgatgctctatttttgttatccaacctcctgcccgctctggcccctaagaggcaccagggactatgttttatctcaccTTACCCAGCGTAGTCTGGGACGTCGTATGGGTATGAGCCGCCTCCGCTCCCTCCGCCgccaaaacctaaccttacaacactcctttccagtgggtaggggtgtg*g*g-3'. For the specific deletion of the S1 cleavage site of OPA1 the following template was used (the 10 amino acids deletion around the S1 cleavage site is marked in **bolt**): c*a*aagaagtaaaaactttaaaaaatctttcaagactacctacatgaacaattctcttttacacttacctttctaaaatgcttgtcactttcttccggagaaccttaaagataaatatgcaaccct*t*t (* marks phosphorothioate bonds). Cas9 RNPs were made by incubating 105 pm Cas9 protein with 120 pmol Alt-R crRNA:tracrRNA duplex in 5 µl volume at 25℃ for 10 min immediately prior to electroporation. $2.5*10^6$ BJAB cells were electroporated using the Lonza Nucleofector 4D and 3.85 µM IDT electroporation enhancer. For HDR-mediated knock-in of the eIF2α S49A S52A variant, 3.7 µM single-stranded oligo DNA nucleotide (ssODN) was added to the electroporation mix. Single clones were obtained by single-cell sorting of electroporated BJAB into 96-well plates and validated by TIDE or ICE (*70*) analysis of single clones to identify homozygous clones.

SUPPLEMENTARY MATERIALS

Materials and Methods

Fig. S1. BTM-3528 and BTM-3566 induces Caspase 3/7 activation in DLBCL cell line but not in the solid tumor cell lines HCT-116 or Hela

Fig. S2. BTM compounds inhibit cell growth and induce G1 cell cycle arrest.

Fig. S3. Pharmacokinetic profile of BTM-3566 in mice

Fig. S4. BTM-3528 induces ATF4 protein expression in a dose-dependent manner.

Fig. S5. Induction of the ATF4 ISR is correlated with reduction in tumor volume *in vivo*

Fig. S6. OMA1 is required for BTM mediated reduction in mitochondrial respiration

Fig. S7. Cell Death in parental and OMA1 -/-; DELE1 -/-; and OPA1ΔS1/ΔS1 genetically modified BJAB cells

Fig S8. Workflow for analyzing the relationship of global gene expression to response of 406 cell lines to BTM-3528.

Fig. S9. Genes correlating with BTM-3528 activity identified using k-fold cross validation.

Figure S10. FAM210B uniquely regulates BTM-3566 mediated ATF4 protein expression in HCT-116 cells

Figure S11. FAM210B overexpression inhibits changes in compound mediated respiration

Figure S12. FAM210B Expression in Normal Blood Cells

Table S1: Cell Line Screening

Table S2: DLBCL Cell Line Screening

Table S3: Crown Screening Data

Table S4: Common genes predictive of response to compound.

Table S5: Biomarker Screening data analysis Spearmans Analysis

Table S6: RNASeq_BTM3528_Data and Analysis

REFERENCES:

1. I. Martínez-Reyes, N. S. Chandel, Cancer metabolism: looking forward. *Nat Rev Cancer*. **21**, 669–680 (2021).

2. M. Li *et al.*, Translational Activation of ATF4 through Mitochondrial Anaplerotic Metabolic Pathways Is Required for DLBCL Growth and Survival. *Blood Cancer Discov*. **3**, 50–65 (2022).

3. K. Vasan, M. Werner, N. S. Chandel, Mitochondrial Metabolism as a Target for Cancer Therapy. *Cell Metab*. **32**, 341–352 (2020).

4. R. J. Deberardinis, A mitochondrial power play in lymphoma. *Cancer Cell*. **22**, 423–424 (2012).

5. J. E. Friedlander *et al.*, Failure to Guard: Mitochondrial Protein Quality Control in Cancer. *Int J Mol Sci*. **22**, 8306 (2021).

6. I. Bohovych, S. S. L. Chan, O. Khalimonchuk, Mitochondrial Protein Quality Control: The Mechanisms Guarding Mitochondrial Health. *Antioxid Redox Signal*. **22**, 977–994 (2015).

7. P. Jadiya, D. Tomar, Mitochondrial Protein Quality Control Mechanisms. *Genes (Basel)*. **11** (2020), doi:10.3390/genes11050563.

8. P. M. Quirós *et al.*, Multi-omics analysis identifies ATF4 as a key regulator of the mitochondrial stress response in mammals. *J. Cell Biol.* **216**, 2027–2045 (2017).

9. A. A. Garaeva *et al.*, Mitochondrial dysfunction induces SESN2 gene expression through Activating Transcription Factor 4. *Cell Cycle*. **15**, 64–71 (2016).

10. J. Ye *et al.*, The GCN2-ATF4 pathway is critical for tumour cell survival and proliferation in response to nutrient deprivation. *EMBO J.* **29**, 2082–2096 (2010).

11. K. Pakos-Zebrucka *et al.*, The integrated stress response. *EMBO Rep.* **17**, 1374–1395 (2016).

12. C. J. Fiorese *et al.*, The Transcription Factor ATF5 Mediates a Mammalian Mitochondrial UPR. *Curr. Biol.* **26**, 2037–2043 (2016).

13. D. Zhou *et al.*, Phosphorylation of eIF2 directs ATF5 translational control in response to diverse stress conditions. *J Biol Chem*. **283**, 7064–7073 (2008).

14. H.-Y. Jiang *et al.*, Activating transcription factor 3 is integral to the eukaryotic initiation factor 2 kinase stress response. *Mol. Cell. Biol.* **24**, 1365–1377 (2004).

15. M. H. Brush, D. C. Weiser, S. Shenolikar, Growth arrest and DNA damage-inducible protein GADD34 targets protein phosphatase 1 alpha to the endoplasmic reticulum and promotes dephosphorylation of the alpha subunit of eukaryotic translation initiation factor 2. *Mol. Cell. Biol.* **23**, 1292–1303 (2003).

16. H. P. Harding *et al.*, Regulated translation initiation controls stress-induced gene expression in mammalian cells. *Mol Cell*. **6**, 1099–1108 (2000).

17. I. Novoa *et al.*, Feedback inhibition of the unfolded protein response by GADD34-mediated dephosphorylation of eIF2alpha. *J Cell Biol*. **153**, 1011–1022 (2001).

18. I. Novoa *et al.*, Stress-induced gene expression requires programmed recovery from translational repression. *EMBO J*. **22**, 1180–1187 (2003).

19. K. D. McCullough *et al.*, Gadd153 Sensitizes Cells to Endoplasmic Reticulum Stress by Down-Regulating Bcl2 and Perturbing the Cellular Redox State. *Mol. Cell. Biol.* **21**, 1249–1259 (2001).

20. P. Gomez-Bougie *et al.*, Repression of Mcl-1 and disruption of the Mcl-1/Bak interaction in myeloma cells couple ER stress to mitochondrial apoptosis. *Cancer Lett.* **383**, 204–211 (2016).

21. N. Hiramatsu *et al.*, Translational and posttranslational regulation of XIAP by eIF2α and ATF4 promotes ER stress-induced cell death during the unfolded protein response. *Mol. Biol. Cell*. **25**, 1411–1420 (2014).

22. R. M. Fritsch *et al.*, Translational repression of MCL-1 couples stress-induced eIF2 alpha phosphorylation to mitochondrial apoptosis initiation. *J Biol Chem*. **282**, 22551–22562 (2007).

23. N. Ohoka *et al.*, TRB3, a novel ER stress-inducible gene, is induced via ATF4-CHOP pathway and is involved in cell death. *EMBO J.* **24**, 1243–1255 (2005).

24. H. Puthalakath *et al.*, ER stress triggers apoptosis by activating BH3-only protein Bim. *Cell*. **129**, 1337–1349 (2007).

25. A. B. Cooper *et al.*, 1-Thiazol-2-yl-N-3-methyl-1H-pyrozole-5-carboxylic acid derivatives as antitumor agents. *Bioorg. Med. Chem. Lett.* **27**, 4471–4477 (2017).

26. L. Plate *et al.*, Small molecule proteostasis regulators that reprogram the ER to reduce extracellular protein aggregation. *Elife*. **5**, e15550 (2016).

27. X. Guo *et al.*, Mitochondrial stress is relayed to the cytosol by an OMA1-DELE1-HRI pathway. *Nature*. **579**, 427–432 (2020).

28. E. Fessler *et al.*, A pathway coordinated by DELE1 relays mitochondrial stress to the cytosol. *Nature*. **579**, 433–437 (2020).

29. S. Ehses *et al.*, Regulation of OPA1 processing and mitochondrial fusion by m-AAA protease isoenzymes and OMA1. *J. Cell Biol.* **187**, 1023–1036 (2009).

30. T. Misaka, T. Miyashita, Y. Kubo, Primary structure of a dynamin-related mouse mitochondrial GTPase and its distribution in brain, subcellular localization, and effect on mitochondrial morphology. *J Biol Chem*. **277**, 15834–15842 (2002).

31. R. Anand *et al.*, The i-AAA protease YME1L and OMA1 cleave OPA1 to balance mitochondrial fusion and fission. *J. Cell Biol.* **204**, 919–929 (2014).

32. B. Head *et al.*, Inducible proteolytic inactivation of OPA1 mediated by the OMA1 protease in mammalian cells. *J. Cell Biol.* **187**, 959–966 (2009).

33. K. Zhang, H. Li, Z. Song, Membrane depolarization activates the mitochondrial protease OMA1 by stimulating self-cleavage. *EMBO Rep.* **15**, 576–585 (2014).

34. M. J. Baker *et al.*, Stress-induced OMA1 activation and autocatalytic turnover regulate OPA1-dependent mitochondrial dynamics. *EMBO J.* **33**, 578–593 (2014).

35. J. Barretina *et al.*, The Cancer Cell Line Encyclopedia enables predictive modelling of anticancer drug sensitivity. *Nature*. **483**, 603–607 (2012).

36. D. Hanahan, R. A. Weinberg, Hallmarks of cancer: the next generation. *Cell*. **144**, 646–674 (2011).

37. E. Giampazolias, S. W. G. Tait, Mitochondria and the hallmarks of cancer. *FEBS J*. **283**, 803–814 (2016).

38. S. J. Marciniak *et al.*, CHOP induces death by promoting protein synthesis and oxidation in the stressed endoplasmic reticulum. *Genes Dev.* **18**, 3066–3077 (2004).

39. H. Yamaguchi, H.-G. Wang, CHOP Is Involved in Endoplasmic Reticulum Stress-induced Apoptosis by Enhancing DR5 Expression in Human Carcinoma Cells. *J. Biol. Chem.* **279**, 45495–45502 (2004).

40. E. V. Maytin *et al.*, Stress-inducible transcription factor CHOP/gadd153 induces apoptosis in mammalian cells via p38 kinase-dependent and -independent mechanisms. *Exp. Cell Res.* **267**, 193–204 (2001).

41. S. Oyadomari, M. Mori, Roles of CHOP/GADD153 in endoplasmic reticulum stress. *Cell Death Differ*. **11**, 381–389 (2003).

42. R. Yamaguchi *et al.*, Opa1-mediated cristae opening is Bax/Bak and BH3 dependent, required for apoptosis, and independent of Bak oligomerization. *Mol Cell*. **31**, 557–569 (2008).

43. C. Frezza *et al.*, OPA1 controls apoptotic cristae remodeling independently from mitochondrial fusion. *Cell*. **126**, 177–189 (2006).

44. R. Yamaguchi, G. Perkins, Dynamics of mitochondrial structure during apoptosis and the enigma of Opa1. *Biochim. Biophys. Acta*. **1787**, 963–972 (2009).

45. R. Gilkerson, P. De La Torre, S. St Vallier, Mitochondrial OMA1 and OPA1 as Gatekeepers of Organellar Structure/Function and Cellular Stress Response. *Front Cell Dev Biol*. **9**, 626117 (2021).

46. M. N. McCall *et al.*, The Gene Expression Barcode 3.0: improved data processing and mining tools. *Nucleic Acids Res*. **42**, D938-943 (2014).

47. Y. Y. Yien *et al.*, FAM210B is an erythropoietin target and regulates erythroid heme synthesis by controlling mitochondrial iron import and ferrochelatase activity. *J. Biol. Chem.* **293**, 19797–19811 (2018).

48. Y. Y. Yien *et al.*, Fam210b Is Required for Optimal Cellular and Mitochondrial Iron Uptake during Erythroid Differentiation. *Blood*. **126**, 405–405 (2015).

49. A. Kondo *et al.*, Identification of a novel putative mitochondrial protein FAM210B associated with erythroid differentiation. *Int. J. Hematol.* **103**, 387–395 (2016).

50. S. Sun *et al.*, Loss of the novel mitochondrial protein FAM210B promotes metastasis via PDK4-dependent metabolic reprogramming. *Cell Death Dis*. **8**, e2870 (2017).

51. M. Uhlén *et al.*, Proteomics. Tissue-based map of the human proteome. *Science*. **347**, 1260419 (2015).

52. A. Yerlikaya, S. R. Kimball, B. A. Stanley, Phosphorylation of eIF2alpha in response to 26S proteasome inhibition is mediated by the haem-regulated inhibitor (HRI) kinase. *Biochem. J.* **412**, 579–588 (2008).

53. H.-Y. Jiang, R. C. Wek, Phosphorylation of the alpha-subunit of the eukaryotic initiation factor-2 (eIF2alpha) reduces protein synthesis and enhances apoptosis in response to proteasome inhibition. *J. Biol. Chem.* **280**, 14189–14202 (2005).

54. J. E. Allen *et al.*, First-In-Class Small Molecule ONC201 Induces DR5 and Cell Death in Tumor but Not Normal Cells to Provide a Wide Therapeutic Index as an Anti-Cancer Agent. *PLoS ONE*. **10**, e0143082 (2015).

55. V. V. Prabhu *et al.*, Single agent and synergistic combinatorial efficacy of first-in-class small molecule imipridone ONC201 in hematological malignancies. *Cell Cycle*. **17**, 468–478 (2018).

56. I. Arrillaga-Romany *et al.*, A phase 2 study of the first imipridone ONC201, a selective DRD2 antagonist for oncology, administered every three weeks in recurrent glioblastoma. *Oncotarget*. **8**, 79298–79304 (2017).

57. X. Ni *et al.*, ONC201 selectively induces apoptosis in cutaneous T-cell lymphoma cells via activating pro-apoptotic integrated stress response and inactivating JAK/STAT and NF-κB pathways. *Oncotarget* (2017) (available at https://www.ncbi.nlm.nih.gov/pubmed/28700333).

58. J. Ishizawa *et al.*, ATF4 induction through an atypical integrated stress response to ONC201 triggers p53-independent apoptosis in hematological malignancies. *Sci. Signal.* **9**, ra17–ra17 (2016).

59. Y. E. Greer, S. Lipkowitz, ONC201: Stressing tumors to death. *Sci. Signal.* **9**, fs1–fs1 (2016).

60. C. L. B. Kline *et al.*, ONC201 kills solid tumor cells by triggering an integrated stress response dependent on ATF4 activation by specific eIF2α kinases. *Sci. Signal.* **9**, ra18–ra18 (2016).

61. A. M. Bolger, M. Lohse, B. Usadel, Trimmomatic: a flexible trimmer for Illumina sequence data. *Bioinformatics*. **30**, 2114–2120 (2014).

62. B. Langmead, S. L. Salzberg, Fast gapped-read alignment with Bowtie 2. *Nat Methods*. **9**, 357–359 (2012).

63. S. Anders, P. T. Pyl, W. Huber, HTSeq--a Python framework to work with high-throughput sequencing data. *Bioinformatics*. **31**, 166–169 (2015).

64. R Core Team, R: A language and environment for statistical computing. *R Foundation for Statistical Computing* (2021) (available at https://www.R-project.org/).

65. W. Huber *et al.*, Orchestrating high-throughput genomic analysis with Bioconductor. *Nat Methods*. **12**, 115–121 (2015).

66. Y. Chen, A. T. L. Lun, G. K. Smyth, From reads to genes to pathways: differential expression analysis of RNA-Seq experiments using Rsubread and the edgeR quasi-likelihood pipeline. *F1000Res*. **5**, 1438 (2016).

67. M. E. Ritchie *et al.*, limma powers differential expression analyses for RNA-sequencing and microarray studies. *Nucleic Acids Res*. **43**, e47 (2015).

68. Y. Benjamini, Y. Hochberg, Controlling the False Discovery Rate: A practical and powerful approach to multiple testing. *Journal of the Royal Statistical Society, Series B (Methodological)*. **57**, 289–300 (1995).

69. A. Subramanian *et al.*, Gene set enrichment analysis: a knowledge-based approach for interpreting genome-wide expression profiles. *Proc Natl Acad Sci U S A*. **102**, 15545–15550 (2005).

70. E. K. Brinkman *et al.*, Easy quantitative assessment of genome editing by sequence trace decomposition. *Nucleic Acids Res*. **42**, e168 (2014).

71. M. E. Torrence *et al.*, The mTORC1-mediated activation of ATF4 promotes protein and glutathione synthesis downstream of growth signals. *eLife*. **10**, e63326 (2021).

ACKNOWLEDGEMENTS:

The authors would like to thank Dr. Josh Rabinowitz of Princeton University and David Weinstock, MD, Merck and Co. for helpful scientific discussions, comments, review and editing of this manuscript. Dr. Alexander van der Bliek, at the UCLA David Geffen School of Medicine UCLA for the HCT-116 OMA 1-/- cell line.

FUNDING:

Bantam Pharmaceutical, Durham, N.C., U.S.

AUTHOR CONTRIBUTIONS:
Conceptualization: MK, MLR, AdS, MH
Methodology: MK, MLR, MO, AdS, MJK, SS, MH, AD, AK, MG, AS
Investigation: MK, MLR, MO, AdS, MJK, SS
Visualization: MK, MLR, MO, AdS
Supervision: MK
Writing – original draft: MK, AdS, MH, MLR

COMPETING INTERESTS:

Adrian Schwarzer: is a member of the Scientific Advisory Board of Bantam Pharmaceutical and received funding in the form of a sponsored research agreement from Bantam Pharmaceuticals.

Anneke Dörrie: no conflict of interest

Matthias Gaestel: no conflict of interest

Marc-Jens Kleppa: no conflict of interest

Alexey Kotlyarov: no conflict of interest

Axel Schambach: no conflict of interest

Marc Liesa: co-founder and consultant of Enspire Bio LLC; received funding in the form of a sponsored research agreement from Bantam Pharmaceuticals.

Linsey Stiles: received contract research funding from Bantam Pharmaceuticals.

Matheus Pinto: no conflict of interest.

Mark Hannink: received funding in the form of a sponsored research agreement from Bantam Pharmaceuticals.

Scott Slattery: received contract research funding from Bantam Pharmaceuticals.

Andy Anantha: is a paid consultant to Bantam Pharmaceutical.

Alan Cooper: is a paid consultant to Bantam Pharmaceutical and is an inventor on patents WO2016196644A1, WO2018102452,WO2018102453, WO2020243582-PAMPH-20201203-0751-1, WO2020243584-PAMPH-20201203-0103 associated with the information in this paper

Todd Hembrough: is a paid consultant to Bantam Pharmaceutical.

Matthew Kostura: is a paid consultant to Bantam Pharmaceutical and is an inventor on patents WO2018102452,WO2018102453 and patent application WO/2019/236936 associated with the information in this paper.

Jedd Levine: is a paid consultant to Bantam Pharmaceutical and is an inventor on patents and is an inventor on patents WO2018102452 and WO2018102453 associated with the information in this paper.

Michael Luther: is an employee of Bantam Pharmaceutical and is an inventor on patents WO2018102452, WO2018102453 and patent application WO/2019/236936 associated with the information in this paper.

Michael Stocum: is an employee of Bantam Pharmaceutical.

DATA AND MATERIALS AVAILABILITY

RNASeq data have been deposited in NCBI's Gene Expression Omnibus. A reviewer access link has been generated and can be obtained from the authors. The R-Code used to perform the bioinformatic analysis is available upon request from the authors. All other data are available in the main text or the supplementary materials. BTM3528 and BTM3566 are available upon request through a materials transfer agreement (MTAs) with Bantam Pharmaceutical.

FIGURES

Fig 1. Pyrazolo-thiazole derivates are novel anti-cancer agents. A) Chemical structures of the BTM pyrazolo-thiazole series. BTM-3528 and BTM-3566 are active versions of the series. BTM-3532 is a closely related inactive member of the series. **B)** BTM-3528 is efficacious in hematopoietic tumor lines. Mean Activity Area of BTM-3528 in 99 tumor cell lines. Tumor tissue of origin and mean activity areas (MAA) are represented on the axes. Increasing activity is shown with increased MAA (greater level of inhibition and more potency IC_{50}. The color of the circle represents the proportion of cell lines found responsive to compound. Circle size represents the number of cell lines screened. **C)** Dose response of tumor cells treated with BTM-3528**.** Left panel are hematopoietic tumor cell lines, right panel are solid tumor lines. **D)** BTM-3528 induces Caspase 3/7 activity in DLBCL cell lines but not solid tumor lines. All data are plotted as the mean (+/- SD, n=3) inhibition in cell growth as compared to vehicle

Fig 2. BTM-3566 induces tumor regression and durable remission in human xenograft models. A) Su-DHL-10 xenograft model: Cells were implanted subcutaneously in the right flank of SCID beige (C.B-17/IcrHsd- Prkdc ^{scid}Lyst^{bg-J}) mice. Tumor volume reached 200 mm^3 prior to randomization into four groups. Mice were then dosed po, qd with vehicle or a solution of 10, 20 or 30 mg/kg BTM-3566 dissolved in 5%NMP/15% Solutol/10% PEG400/70% D5W. Top Panel: Tumor volume, Bottom Panel: body weights were determined every 3 days. The vertical line at day 21 represents the end of drug dosing. All data are the mean +/- SD (n=10 animals). B) BTM-

3566 is efficacious in human PDX models. Nine human DLBCL PDX tumors were implanted into scid mice. All groups received drug or vehicle for 21 days. Treatment arms received BTM-3566, 20 mg/kg, po, qd.Tumor volume was measured and recorded every other day. All data represented as mean ± SD (n=3 animals). •=Vehicle; •= BTM-3566. C) Tabulated result of PDX model testing. CR, Complete Response, no palpable tumor; PR, Partial Response with palpable tumor lower than baseline; SD, Stable Disease, tumor volume is not increased above baseline; PD, Progressing Disease where tumor is larger than starting tumor volume.

Fig. 3. BTM-3528 activates the ATF4-linked mitochondrial stress response A) Volcano plots showing the adjusted P-value ($-\log_{10}$ P) versus the fold change (log2) for 14,287 genes after 2,4,6, and 8 hrs. of treatment with BTM-3528 versus vehicle. The dashed lines indicate the log2-FC cutoff =1.0 and the adj.p-value cutoff = 10^{-3}. ATF4-target genes *(71)* are written in red font. **B)** Gene Set Enrichment Analysis (GSEA) of 1773 canonical pathway gene sets from MSigDB C2 of BTM-3528 treated samples versus controls at 8 hrs. Plotted are normalized enrichment scores (NES) against the false discovery rate (FDR). The enrichment cutoff (FDR < 0.05) is indicated by the dashed line. **C)** Gene set enrichment analysis for the ATF6 target genes (left panel), XBP1s target genes (middle panel) *(26)* and the mitostress signature (right panel) *(8)* in HCT116 cells treated with BTM3528 for 8 hrs. **D)** qPCR analysis of a panel of cell lines treated with BTM-3528 for 8 hours. Lower panel shows gene changes expressed as log2 fold change compared to vehicle (n=3). Upper panel shows the -LogP value for each triplicate sample as compared to vehicle. **E)** Immunoblot of phosphorylated eIF2α in HCT-116 following treatment with BTM-3528. for the indicated time. **F)** Dose response of nuclear ATF4 protein abundance in HCT-116 cells treated with BTM3528 for the indicated time and dose. **G)** Immunoblot of phosphorylated eIF2*α* and ATF4 in BJAB cells treated with 2 μM BTM-3528 for 3 hrs.

Fig. 4. BTM compound treatment fragments the mitochondria and induces OPA1 cleavage in an OMA1 dependent manner. A) Representative images from HCT116 cells stained with mitotracker green (MTG) and imaged using confocal laser microscopy. **B)** Mitochondrial Aspect Ratio and Form factor are reduced following treatment with BTM-3528. Aspect Ratio and Form Factor are the average of 4 independent experiments, n= 5 cells and 50 – 70 mitochondria identified per cell, t-test, ***, P<.005) **C)** Mitochondrial Membrane Potential in HCT-116 cells treated with 3 μM BTM-3532, BTM-3528 and BTM-3566 for 4 hours then stained with TMRE and MTG. All

images were quantified using merged channels indicating colocalization of the TMRE and MTG pixels. FCCP is a used as a positive control. **(D-E)** Representative Western blot analysis and quantification of BTM compound induced OPA-1 long forms (L) cleavage to short isoforms (S). HCT-116 Parental cells () and HCT-116 0MA1 -/- treated for 4 hours with BTM compounds; Bar graph plotted as the average +/- SEM, n=3. ****p<0.0001. **(F, G)** Western blot analysis and quantification of the ratio of the GAPDH normalized L1 OPA-1 to L2 isoforms in parental HCT-116 cells treated with compound for 30 minutes. Bar graph plotted as the Standardized Score calculated for each experiment. ** p<.005 (n=3) **H)** Respirometry of HCT-116 cells treated with compounds for 30 minutes. All data are plotted as the mean +/- SD (n=3) **I)** Quantitation of the Basal, ATP linked and uncoupled OCR rates and **J)** Bioenergetic efficiency in HCT-116 parental and OMA1 -/- cells. All data are the mean +/- SD, n=3, *, p<.01

Fig 5. BTM compounds induce the ATF4 ISR via the OMA1-DELE1 mitochondrial quality control pathway. A) Model of OMA1 mediated induction of the ATF4 ISR. **B)** Western Blot analysis of OMA1, OPA1, phospho-eIF2□ and ATF4 in BJAB parental, OMA1 -/-, DELE1 -/-,; and OPA1ΔS1/ΔS1 genetically modified cells following 4 hours of treatment with vehicle or 2 μM BTM-3566. **C)** Cell Death in parental and OMA1 -/-; DELE1 -/-; and OPA1DS1/DS1 genetically modified BJAB cells following treatment with 2 μM BTM-3566. Annexin-Propidium Iodide staining of cells at 12, 24 and 48 hours of exposure. All data are plotted as the mean +/- SD (n=3). **D)** Western Blot analysis of phospho-eIF2α and ATF4 levels in BJAB parental, HRI -/-; eIF2α Ser49/Ser52 mutant and ATF4 -/- genetically modified cells following 4 hours of treatment with vehicle or 2 μM BTM-35*66*. **E)** Cell Death in parental and HRI -/- and eIF2α Ser49/Ser52 mutant genetically modified cells following treatment with 2 μM BTM-35*66*. Annexin-Propidium Iodide staining of cells at 12, 24 and 48 hours of exposure. All data are plotted as the mean +/- SD (n=3). *(F-I)* Polysome profiles of parental (*F*)*; HRI -/- (G);* eIF2α mutant (*H*) and ATF4 -/- cells (I) treated with 2 μM BTM-35*66* (blue line = vehicle; gold line = 4 hrs. treatment with BTM-3528).

Fig. 6. FAM210B mRNA expression is correlated with and regulates cellular response to BTM compounds. A) Correlations of AUC to gene expression across 284 cell lines are expressed as the Spearman's correlation coefficient vs the -LogP value for each gene. B) Cell lines (n=284) were classified as responder (AUC > 3.25) or non-responder (AUC < 3.25) *** p<.001. • Solid tumor lines; • Hematopoietic tumor lines; • BCL Lines. C) Waterfall plot of FAM210B mRNA expression data for screened cell lines. Data are plotted by descending standardized FAM210B

expression level. D) Parental, FAM210BtGFP or HRI -/- BJAB cells were tested for sensitivity to BTM-3528, BTM-3566, BTM-3532, Bortezomib and FCCP. Cell death was determined by Annexin and YOYO staining. E) OPA1 cleavage was determined in HCT-116 parental and FAM210BtGFP cells following a 3-hour treatment with 3 μM BTM compounds.

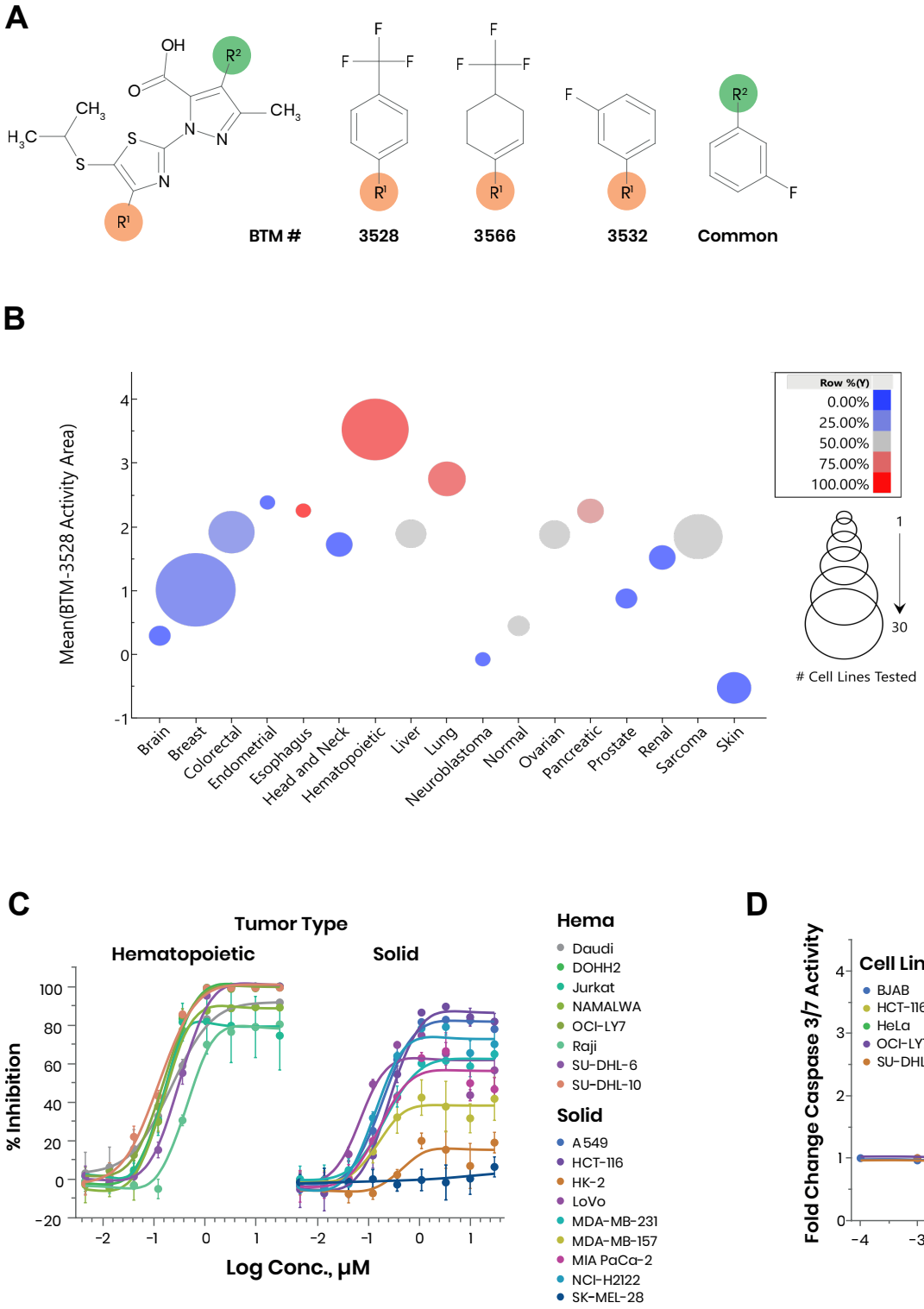
A
OH
O
R2
CH3
CH3
H3C
S
S
N
N
N
R1
BTM #
3528
3566
3532
Common
F
F
F
R2
B
Mean(BTM-3528 Activity Area)
Brain
Breast
Colorectal
Endometrial
Esophagus
Head and Neck
Hematopoietic
Liver
Lung
Neuroblastoma
Normal
Ovarian
Pancreatic
Prostate
Renal
Sarcoma
Skin
Row %(Y)
0.00%
25.00%
50.00%
75.00%
100.00%
1
30
Cell Lines Tested
C
Tumor Type
Hematopoietic
Solid
% Inhibition
Log Conc., μM
Hema
Daudi
DOHH2
Jurkat
NAMALWA
OCI-LY7
Raji
SU-DHL-6
SU-DHL-10
Solid
A549
HCT-116
HK-2
LoVo
MDA-MB-231
MDA-MB-157
MIA PaCa-2
NCI-H2122
SK-MEL-28
D
Fold Change Caspase 3/7 Activity
Cell Line
BJAB
HCT-116
HeLa
OCI-LY7
SU-DHL-10
Log Conc., μM

A

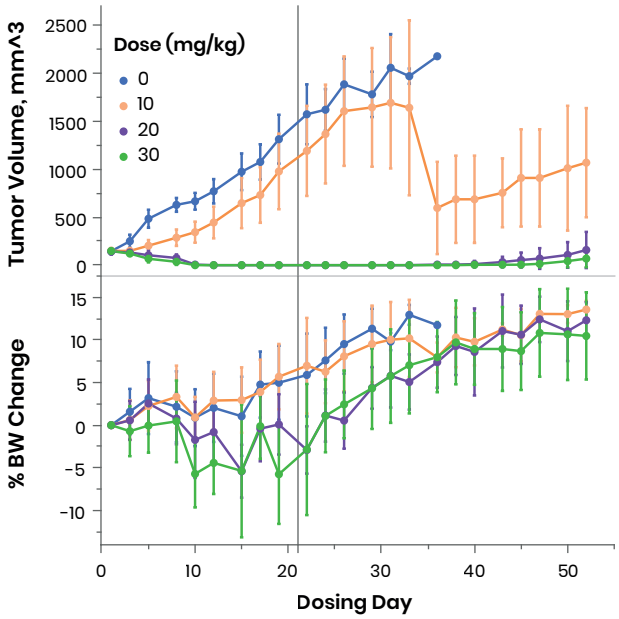

B

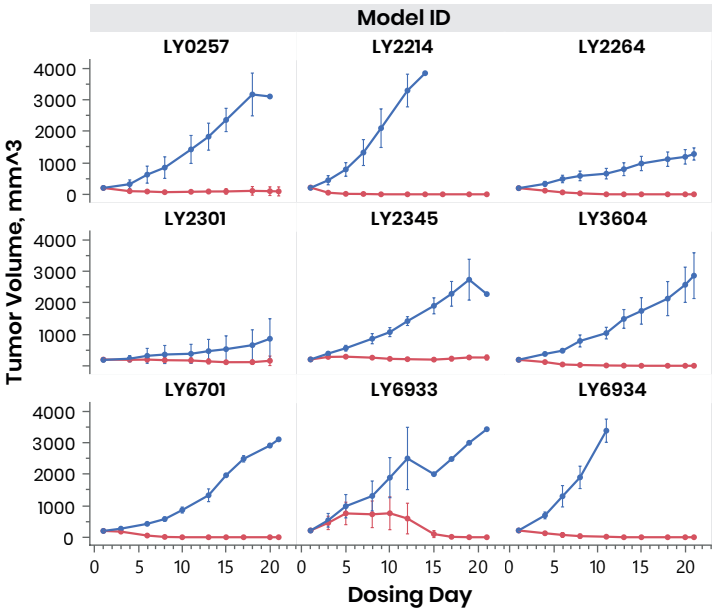

C

PDX Model		Response, Day 21				
Model ID	Genotype	% TGI	CR	PR	SD	PD
LY0257	ABC, MYD88, L2656P	97	1	1	1	
LY2214	GCB	100	3			
LY2264	ABC, MYD88, L2656P	100	3			
LY2301	ABC	89		2		1
LY2345	ABC/GCB	100		1	1	1
LY3604	ABC/GCB	100	3			
LY6701	GCB	100	3			
LY6933	ABC/GCB	100	3			
LY6934	ABC/GCB	100	3			

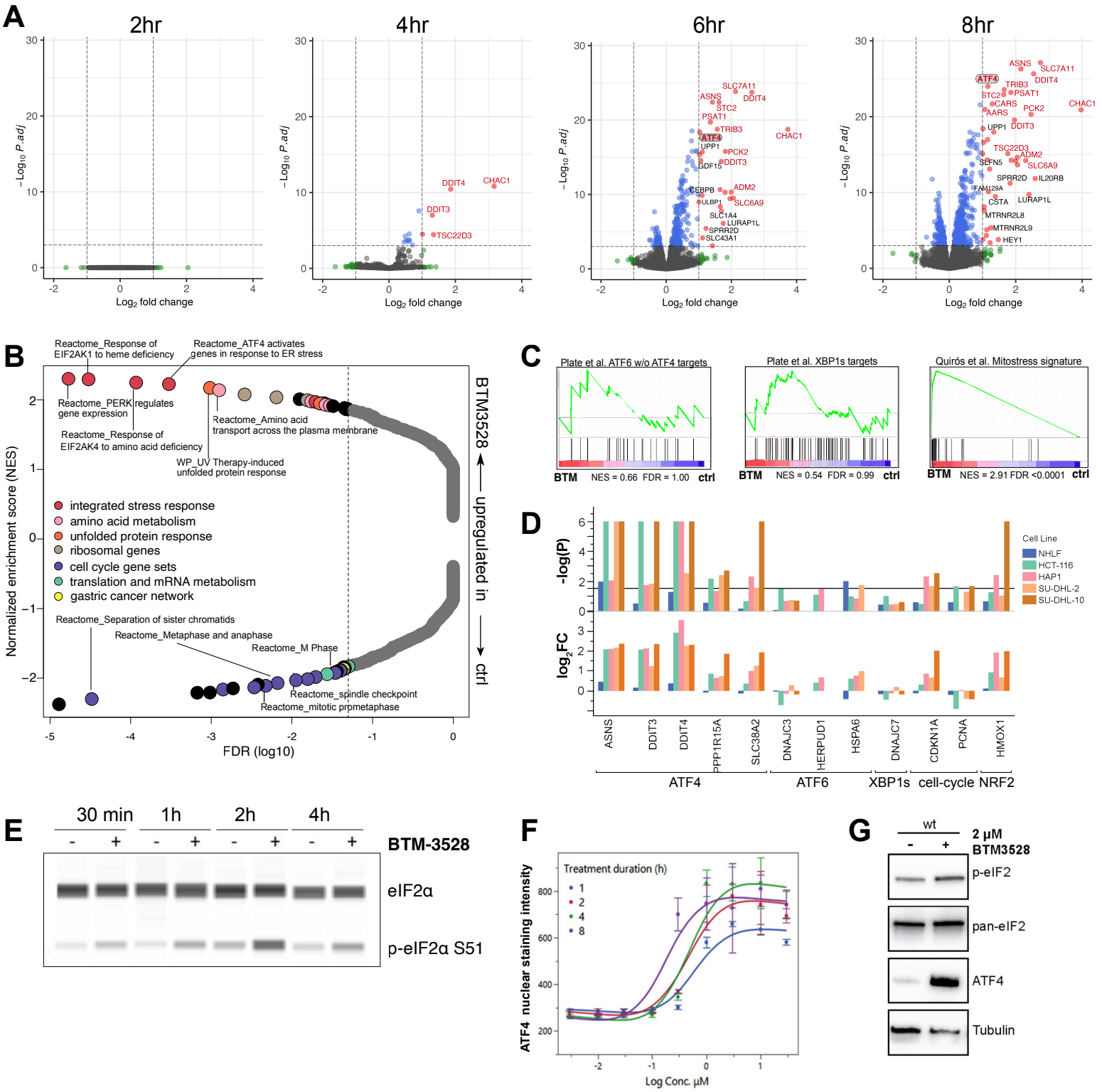
A
2hr
4hr
6hr
8hr
−Log10 P.adj
Log2 fold change
DDIT4
CHAC1
DDIT3
TSC22D3
ASNS
SLC7A11
STC2
PSAT1
TRIB3
ATF4
UPP1
PCK2
GDF15
CEBPB
ADM2
ULBP1
SLC6A9
SLC1A4
LURAP1L
SPRR2D
SLC43A1
B
Reactome_Response of EIF2AK1 to heme deficiency
Reactome_ATF4 activates genes in response to ER stress
Reactome_PERK regulates gene expression
Reactome_Response of EIF2AK4 to amino acid deficiency
Reactome_Amino acid transport across the plasma membrane
WP_UV Therapy-induced unfolded protein response
integrated stress response
amino acid metabolism
unfolded protein response
ribosomal genes
cell cycle gene sets
translation and mRNA metabolism
gastric cancer network
Reactome_Separation of sister chromatids
Reactome_Metaphase and anaphase
Reactome_M Phase
Reactome_spindle checkpoint
Reactome_mitotic prometaphase
Normalized enrichment score (NES)
FDR (log10)
BTM3528
upregulated in
ctrl
C
Plate et al. ATF6 w/o ATF4 targets
Plate et al. XBP1s targets
Quirós et al. Mitostress signature
BTM NES = 0.66 FDR = 1.00 ctrl
BTM NES = 0.54 FDR = 0.99 ctrl
BTM NES = 2.91 FDR <0.0001 ctrl
D
-log(P)
log2FC
Cell Line
NHLF
HCT-116
HAP1
SU-DHL-2
SU-DHL-10
ASNS
DDIT3
DDIT4
PPP1R15A
SLC38A2
DNAJC3
HERPUD1
HSPA6
DNAJC7
CDKN1A
PCNA
HMOX1
ATF4
ATF6
XBP1s
cell-cycle
NRF2
E
30 min
1h
2h
4h
BTM-3528
eIF2α
p-eIF2α S51
F
Treatment duration (h)
ATF4 nuclear staining intensity
Log Conc. μM
G
wt
2 μM BTM3528
p-eIF2
pan-eIF2
ATF4
Tubulin

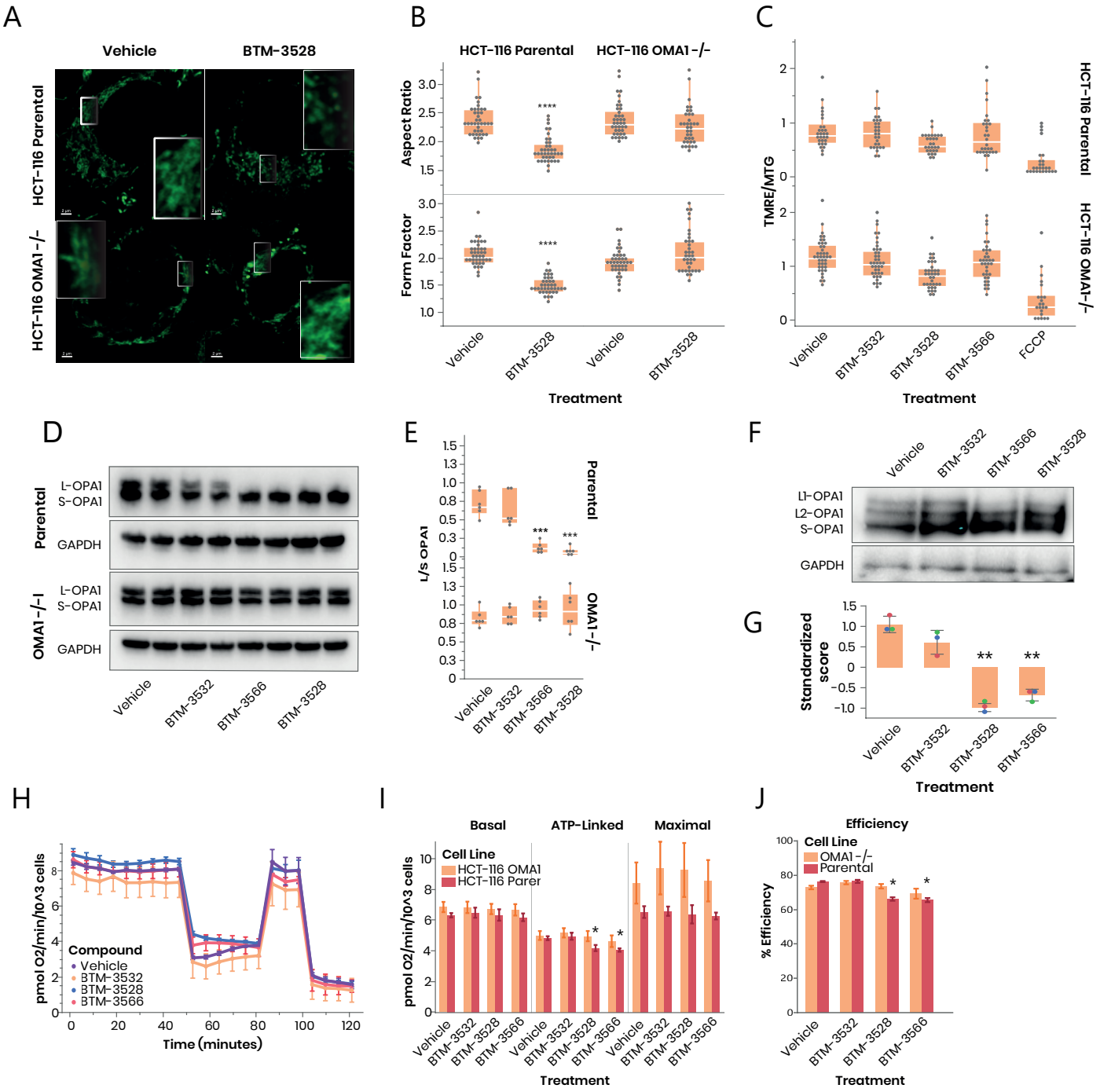
A
Vehicle
BTM-3528
HCT-116 Parental
HCT-116 OMA1 -/-
B
HCT-116 Parental
HCT-116 OMA1 -/-
Aspect Ratio
Form Factor
****
Vehicle
BTM-3528
Treatment
C
TMRE/MTG
HCT-116 Parental
HCT-116 OMA1-/-
Vehicle
BTM-3532
BTM-3528
BTM-3566
FCCP
Treatment
D
Parental
L-OPA1
S-OPA1
GAPDH
OMA1 -/-l
Vehicle
BTM-3532
BTM-3566
BTM-3528
E
L/S OPA1
Parental
OMA1 -/-
***
F
L1-OPA1
L2-OPA1
S-OPA1
GAPDH
G
Standardized score
**
Treatment
H
pmol O2/min/10^3 cells
Compound
Vehicle
BTM-3532
BTM-3528
BTM-3566
Time (minutes)
I
Basal
ATP-Linked
Maximal
Cell Line
HCT-116 OMA1
HCT-116 Parer
*
Treatment
J
Efficiency
Cell Line
OMA1 -/-
Parental
% Efficiency
Treatment

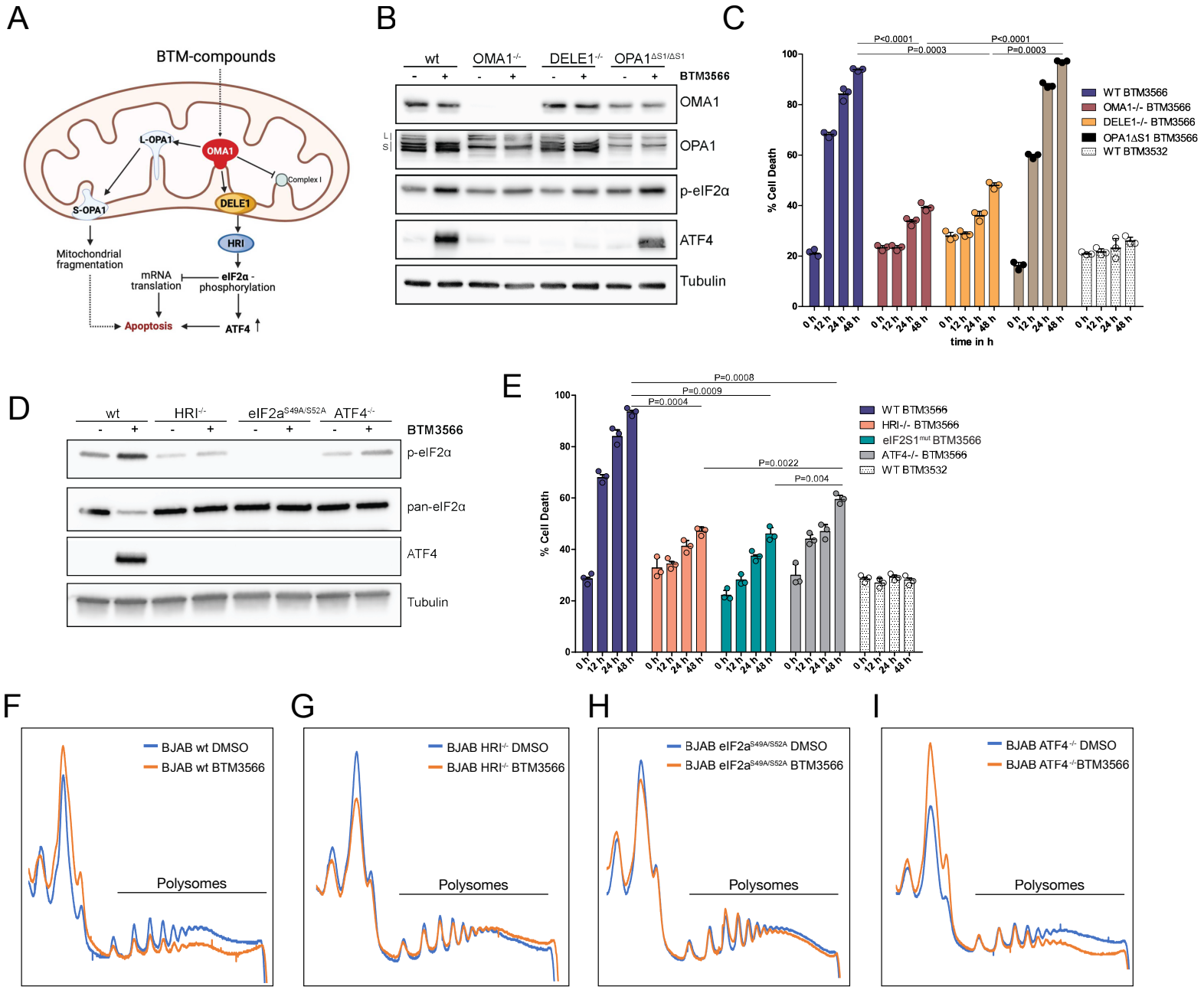
A
BTM-compounds
L-OPA1
OMA1
Complex I
S-OPA1
DELE1
HRI
Mitochondrial fragmentation
mRNA translation
eIF2α - phosphorylation
Apoptosis
ATF4
B
wt
OMA1-/-
DELE1-/-
OPA1ΔS1/ΔS1
BTM3566
OMA1
OPA1
L
S
p-eIF2α
ATF4
Tubulin
C
P<0.0001
P<0.0001
P=0.0003
P=0.0003
% Cell Death
time in h
WT BTM3566
OMA1-/- BTM3566
DELE1-/- BTM3566
OPA1ΔS1 BTM3566
WT BTM3532
D
wt
HRI-/-
eIF2aS49A/S52A
ATF4-/-
BTM3566
p-eIF2α
pan-eIF2α
ATF4
Tubulin
E
P=0.0008
P=0.0009
P=0.0004
P=0.0022
P=0.004
% Cell Death
WT BTM3566
HRI-/- BTM3566
eIF2S1mut BTM3566
ATF4-/- BTM3566
WT BTM3532
F
BJAB wt DMSO
BJAB wt BTM3566
Polysomes
G
BJAB HRI-/- DMSO
BJAB HRI-/- BTM3566
Polysomes
H
BJAB eIF2aS49A/S52A DMSO
BJAB eIF2aS49A/S52A BTM3566
Polysomes
I
BJAB ATF4-/- DMSO
BJAB ATF4-/-BTM3566
Polysomes

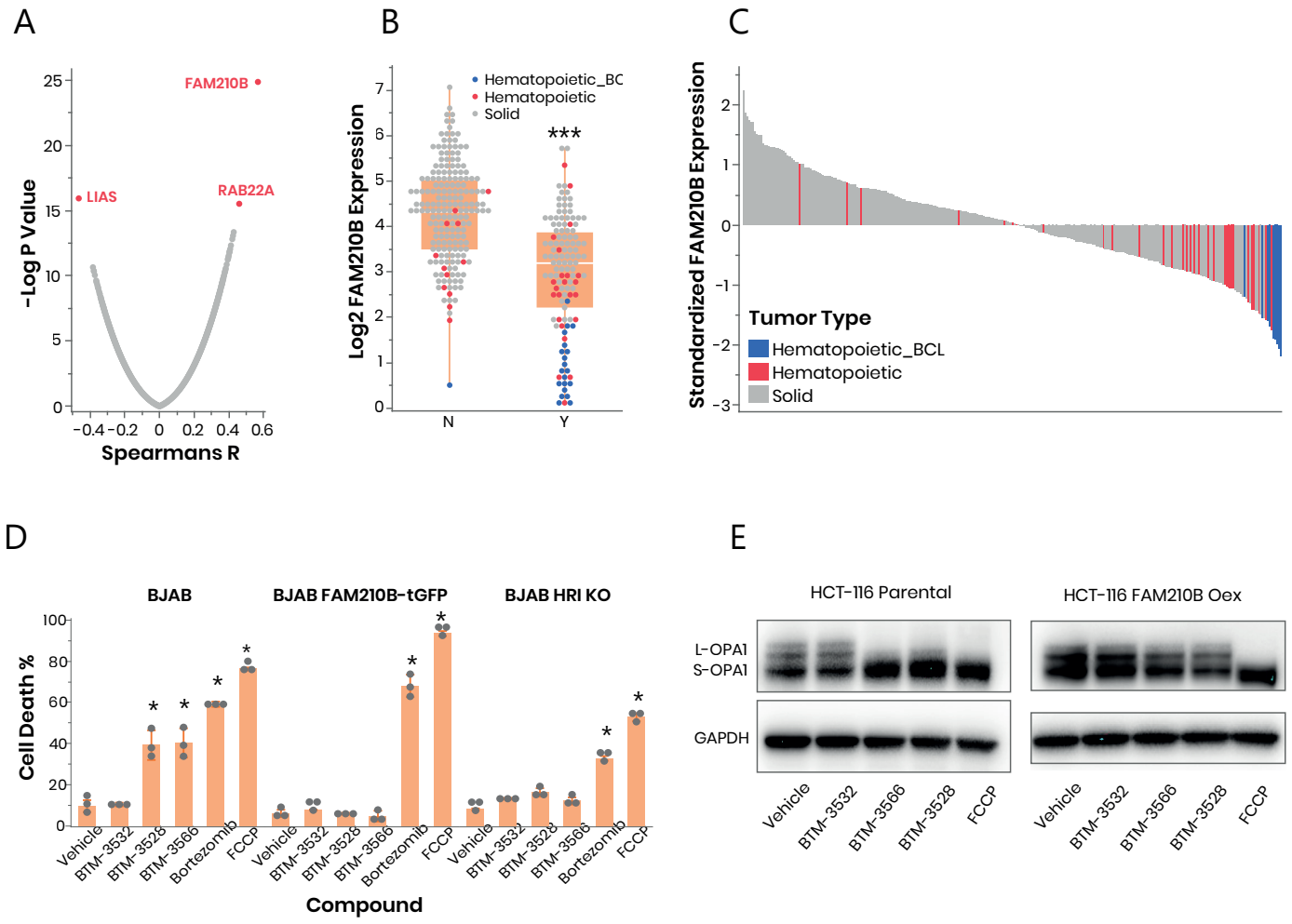
A
FAM210B
LIAS
RAB22A
-Log P Value
Spearmans R
B
Hematopoietic_BC
Hematopoietic
Solid
***
Log2 FAM210B Expression
N
Y
C
Standardized FAM210B Expression
Tumor Type
Hematopoietic_BCL
Hematopoietic
Solid
D
BJAB
BJAB FAM210B-tGFP
BJAB HRI KO
Cell Death %
Vehicle
BTM-3532
BTM-3528
BTM-3566
Bortezomib
FCCP
Compound
E
HCT-116 Parental
HCT-116 FAM210B Oex
L-OPA1
S-OPA1
GAPDH
Vehicle
BTM-3532
BTM-3566
BTM-3528
FCCP